Variable optical attenuator based on photonic crystal waveguide with low-group-index tapers

Qiang Zhao, Kaiyu Cui,* Xue Feng, Fang Liu, Wei Zhang, and Yidong Huang

Department of Electronic Engineering, National Laboratory for Information Science and Technology,
Tsinghua University, Beijing 100084, China

*Corresponding author: kaiyucui@tsinghua.edu.cn

We demonstrate a compact thermo-optic variable optical attenuator (VOA) based on the cutoff effect of W1 photonic crystal waveguide (PCW). In experiment, a variable attenuation range of 29 dB is achieved with a device length of only 16.8 μm. The coupling loss is also reduced by 7.5 ± 2.5 dB through introducing low-group-index tapers between the W1 PCW and strip waveguide. This VOA provides the largest variable attenuation range in the reported tunable PCW device to our knowledge.   © 2013 Optical Society of America

OCIS codes: (130.3120) Integrated optics devices; (230.5298) Photonic crystals.
http://dx.doi.org/10.1364/AO.52.006245

1. Introduction

A variable optical attenuator (VOA) is an essential device in a photonic integrated circuit (PIC) for channel power equalizing in wavelength division multiplex technology. The VOA function can be achieved by many different structures, including microelectromechanical systems [1,2], planar light wave circuits [3–5], microfluidics [6], and tunable silicon photonic devices. Among them, the silicon photonic devices are particularly attractive due to the compatibility with standard complementary metal oxide semiconductor processes. Meanwhile, high integration density can be achieved with high refractive index contrast between silicon and silica. However, the conventional silicon photonic VOAs are based on Mach–Zehnder interferometer structure or silicon electric absorption structure, which are both with millimeter-level sizes [7,8]. To meet the growing demands of the integration level for PICs, more compact VOAs are required.

A promising solution of compact optical devices is introducing line-defect photonic crystal waveguides (PCWs) with slow light enhancement [9,10], which has been widely used to realize compact devices, such as modulators and switches in tens of micrometers [11–18]. Moreover, the slow light effect in PCWs can lead to transmission cutoff [19–21], which performs as a sharp band edge in transmission spectrum. Previously, we have realized the VOAs by the cutoff effect of slow light with a variable attenuation range of only 10 dB [22]. In this paper, we demonstrate a 16.8-μm-long VOA based on the cutoff effect of the W1 PCW to reduce the additional insertion loss and enlarge variable attenuation range. In experiment, we introduce five-period-long W1.2 low-group-index (LGI) tapers between the W1 PCW and strip waveguide to enhance the coupling efficiency [18] and reduce the insertion loss of 7.5 ± 2.5 dB in the slow light region. The measured variable attenuation range is 29 dB, and the power consumption is less than 43 mW. This VOA provides the largest variable attenuation range in the reported tunable PCW device to our knowledge, and the device length is only 1% of those of the traditional on-chip VOAs.

2. Device Structure and Principle

The VOA is formed by a line-defect silicon PCW and an integrated titanium/aluminum (Ti/Al) microheater,
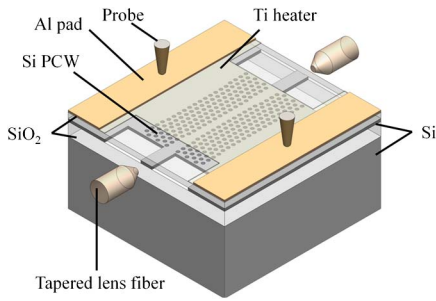
Fig. 1. Schematic of the VOA.

as shown in Fig. 1. The PCW is fabricated on silicon-on-insulator (SOI) substrate with 220-nm-thick Si layer, and insulated from the microheater by 600-nm-thick SiO$_2$ cladding. The microheater consists of a 100-nm-thick Ti heating strip and 300-nm-thick Al contact pads, and the Ti strip is located right above the PCW. The sizes for the PCW and the Ti heater are 16.8 μm × 8 μm and 15 μm × 14 μm, respectively [16,17].

The VOA contains slow light PCW, LGI tapers, and strip waveguides, as presented in Fig. 2. Here we use W to express the line-defect width of the PCW, as

$$W = (x + 1) \times (\sqrt{3}/2)a, \qquad (1)$$

where a is the lattice period and x can be set for certain width [17]. Thus, the PCW with different line-defect widths can be denoted as Wx, such as the typical W1 and W3 PCW with line-defect widths of one and three rows of missing holes for $x = 1$ and 3, respectively. The LGI tapers are introduced between the PCW and the strip waveguides to reduce the coupling loss of slow light. The line-defect width of the slow light PCW and LGI tapers are set as W_{PCW} and W_{Taper}, and the width of the strip waveguide is also set as W_{Taper} for improving coupling efficiency [17]. The line-defect width of the LGI taper (W_{Taper}), as well as the strip width, are larger than that of the slow light PCW (W_{PCW}), while the lattice period and hole radius remain the same [23].

We illustrate the principle of the VOA function by dispersion curves and transmission spectra of the W1 PCW, which are calculated by the two-dimensional plane wave expansion method with an effective refractive index of $n_{eff} = 2.71$ and the three-dimensional (3D) finite-difference time-domain (FDTD) method
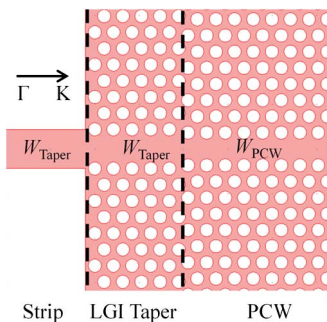
Fig. 2. PCW and LGI taper structure.

with the refractive index of $n_{Si} = 3.43$, respectively. The refractive index of SiO$_2$ is 1.45 in simulation. The ratio of the hole radius and lattices period of the W1 PCW is $r/a = 137$ nm/420 nm, and the device length is $40a$. The dispersion curves and transmission spectra of the W1 PCW for TE polarization is shown in Fig. 3. Due to the line-defect of PCW, two defect modes are introduced to the bandgap area, including a fundamental mode (zero-order,) and a first-order mode. The dispersion curve of the fundamental mode becomes more and more flat and shows a cutoff near the boundary of the first Brillouin zone, which means the group velocity of the fundamental mode, defined as the slope of the dispersion curve ($V_g = d\omega/dk$), becomes smaller when approaching the cutoff frequency. The cutoff frequency, as well as the dispersion curves, shifts to red when the silicon refractive index increases. This effect leads to a transmission drop shift in transmission spectra, as shown in Fig. 3(b).

The VOA function is achieved by shifting the transmission spectrum through thermo-optic effect with a thermo-optic coefficient of $\Delta n/\Delta T = 1.86 \times 10^{-4}$ K^{-1} for silicon. According to the silicon thermo-optic effect, the cutoff wavelength can be shifted by changing the temperature of the integrated microheater [24]. When applying different heating power, the transmission spectra shift, so that the attenuation at the operating wavelength varies. The insertion loss noted in Fig. 3(b) is defined as the peak power of transmitted light at the edge of the cutoff. The attenuation is the transmission drop from the peak power to the transmission power at the operating wavelength, as seen in Fig. 3(b).

The refractive index shift of 0.03 in PCWs corresponds to a temperature shift of 161 K, and the temperature shifts transferred from microheater to the PCW is calculated by applying the 3D finite element analysis method [17], as presented in Fig. 4. The simulated heating transfer efficiency, η, defined as $\Delta T_{PCW}/\Delta T_{Microheater}$ is 72%, which indicates that the temperature shift on the microheater is 224 K.

PCWs with different line-defect widths (Wx) and r/a cause different insertion loss and variable attenuation range, which are presented in Figs. 5(a)
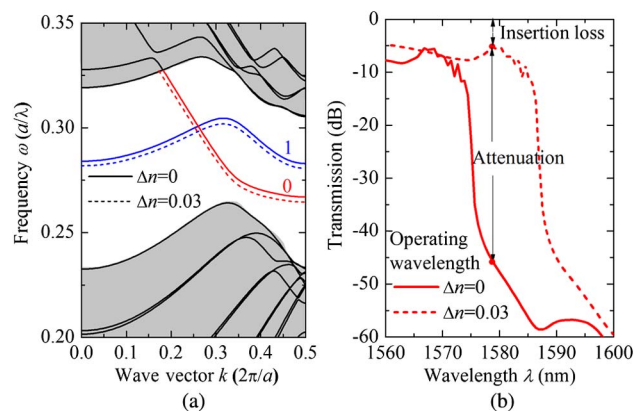
Fig. 3. (a) Dispersion curve and (b) transmission spectra shift of the W1 PCW.
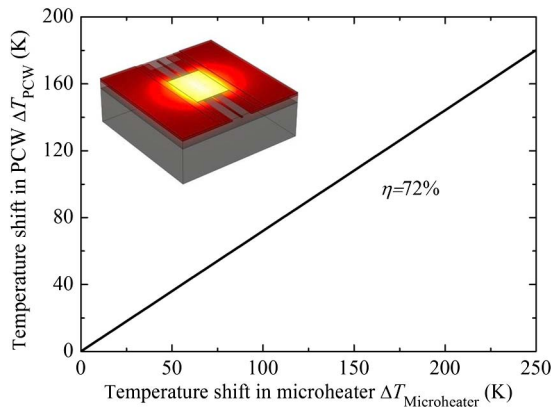
Fig. 4. Temperature shifts transferred from microheater to PCW.

and 5(b). The r/a and x change from 0.28 to 0.38 and 0.6 to 1.1, respectively, while the device length is fixed at $40a$. Figure 5(a) shows a negative correlation between the insertion loss and the line-defect width, as the wider line-defect has higher coupling efficiency between the strip waveguide and the PCW. The calculation results also show that smaller insertion loss is achieved with smaller ratio of r/a. The variable attenuation range is affected by both transmission drop depth and insertion loss. For line-defect width Wx with $x < 1$, the cutoff effect leads to the transmission drop. The transmission drop depth for PCWs with the same r/a and length is at the same level, since the bandgap structure of PCWs is mainly affected by the ratio of r/a. Thus the variable attenuation range is negatively correlated to the insertion loss and positively correlated to the line-defect width. For line-defect width Wx with $x > 1$, although wider line-defect results in lower insertion loss, the cutoff effect happens only when the line-defect width satisfies the single-mode transmission conditions at the cutoff wavelength, since the cutoff effect will disappear due to the mode coupling between the fundamental mode and higher-order modes [16,17]. In summary, in order to obtain small insertion loss and large variable attenuation range, $x = 1$ and $r/a \sim 0.32$ should be chosen.

Compared with transmission loss, the insertion loss is mainly caused by coupling loss for short PCWs. To reduce the insertion loss, LGI tapers are introduced to enhance the coupling efficiency in the slow light region [18,23,25,26]. A simple and efficient way to design the LGI taper is broadening the line-defect width of the PCW while the lattice period and the hole radius remain the same [18]. Here, we first calculate the group index (inversely proportional to the group velocity) of the PCW with different line-defect width, as shown in Fig. 6(a). It can be seen that when 1550 nm $< \lambda <$ 1575 nm, the W1 PCW presents

Fig. 5. Distributions of (a) insertion loss and (b) extinction ratio of the PCWs with different ratio of radius/lattice period (r/a) and line-defect width.
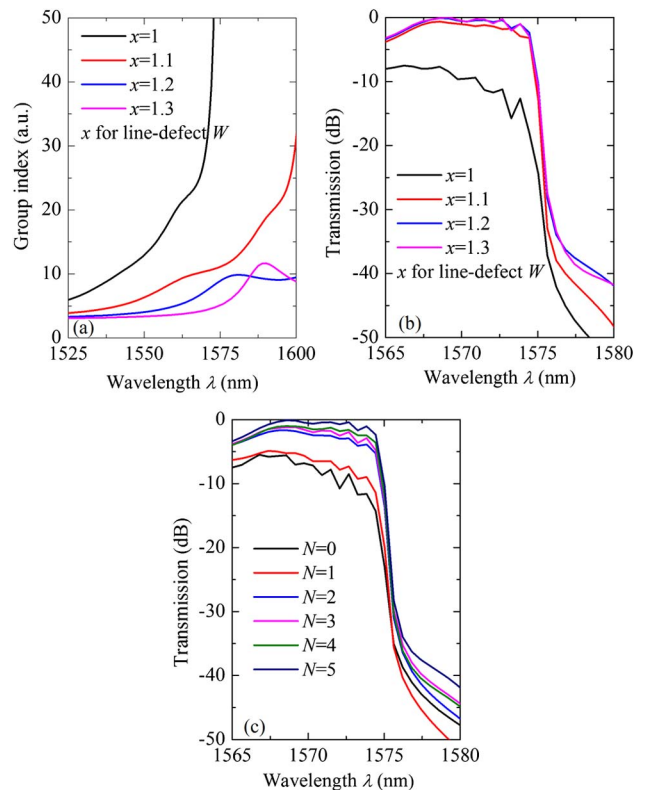
Fig. 6. Simulated (a) group index, (b) transmission spectra of the original W1 PCW and with different line-defect width (x for line-defect width W) of the LGI tapers, and (c) transmission spectra of the original W1 PCW with different lattice period number (N) of the W1.2 LGI taper.

a larger group index, corresponding to the slow light region, while the PCW with line-defect width larger than W1 remains with low group index. Thus, the coupling becomes more efficient, as shown in Fig. 6(b), and the insertion loss is reduced by 7 ± 3 dB after introducing the LGI taper. Further broadening of the line-defect of LGI tapers to wider than W1.2 will not markedly enhance the coupling efficiency between the W1 PCW and the strip waveguide, since the group index cannot be reduced below the normal level [23]. Then we calculate the transmission spectra of the W1 PCW with different lengths of the W1.2 LGI taper, as presented in Fig. 6(c). From 3D FDTD simulation we found that the W1.2 LGI taper for a small number of period $(N > 1)$ becomes efficient, and exploiting the five-period-long W1.2 LGI tapers can reduce the insertion loss to less than 0.1 dB.

3. Experiment

The VOAs based on W1 PCW without and with LGI tapers are fabricated and the optical microscope image of the fabricated VOA sample is shown in Fig. 7(a). The PCW pattern is defined on a SOI wafer by electron beam lithography using ZEP-520 resist and inductively coupled plasma dry etching. Then, a SiO$_2$ layer is deposited by plasma-enhanced chemical vapor deposition on the PCW to insulate the Ti/Al microheater. After depositing SiO$_2$, the microheater is formed by photoetching and evaporating Ti/Al metal. The Ti heater is a 14 μm × 15 μm slab and located right above the W1 PCW. Figure 7(b) presents the scanning electron microscope image of the W1 PCW with five-period-long W1.2 LGI tapers on both ends. The parameters of W1 PCW and LGI tapers are $r/a = 135$ nm/420 nm, and the total length of the PCW is $40a$, i.e., 16.8 μm.

The transmission spectra of the fabricated VOAs are measured by an autoalignment coupling system. The input light is coupled from a tunable laser with a TE polarization. The optical signal is coupled into/out of the VOA through a pair of tapered lens fibers, and the electrical signal is applied on the VOA by two electrical probes.

To verify the enhancement of LGI tapers in coupling, we measured the transmission spectra of the tapered and original W1 PCW, and the results are shown in Fig. 8. With the W1.2 LGI tapers, the coupling efficiency does not decay markedly near the band edge as the original W1 PCW, and the insertion
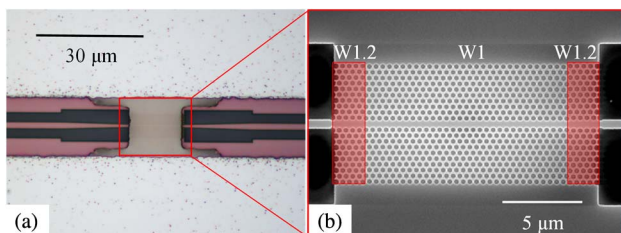
Fig. 7. (a) Optical microscope image of the fabricated VOA and (b) scanning electron microscope image of the W1 PCW with W1.2 LGI tapers.
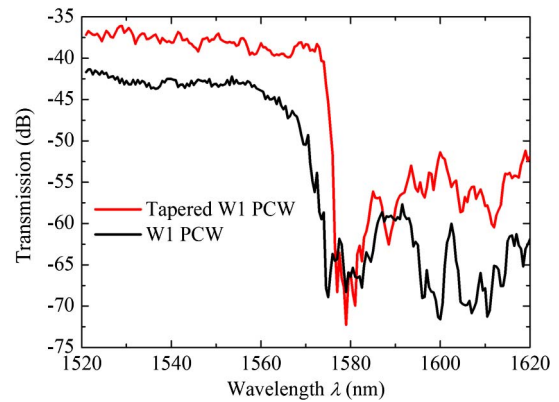
Fig. 8. Measured transmission spectra of the original W1 PCW and W1 PCW with five-period-long W1.2 LGI tapers.

loss is reduced by 7.5 ± 2.5 dB. Here, the little difference of cutoff wavelength between the tapered and original W1 PCW is due to the fabrication deviation of the small hole radius.

The characteristic of the VOA is measured by applying different voltage on the Al pad. The measured transmission spectra redshift with applied voltage of 2 V is shown in Fig. 9(a). Accordingly, the attenuation at the cutoff wavelength of 1577 nm keeps on decreasing when the applied voltage increases, and a variable attenuation range of 29 dB is achieved by a maximum voltage of 2.2 V, as noted in Fig. 9(b).
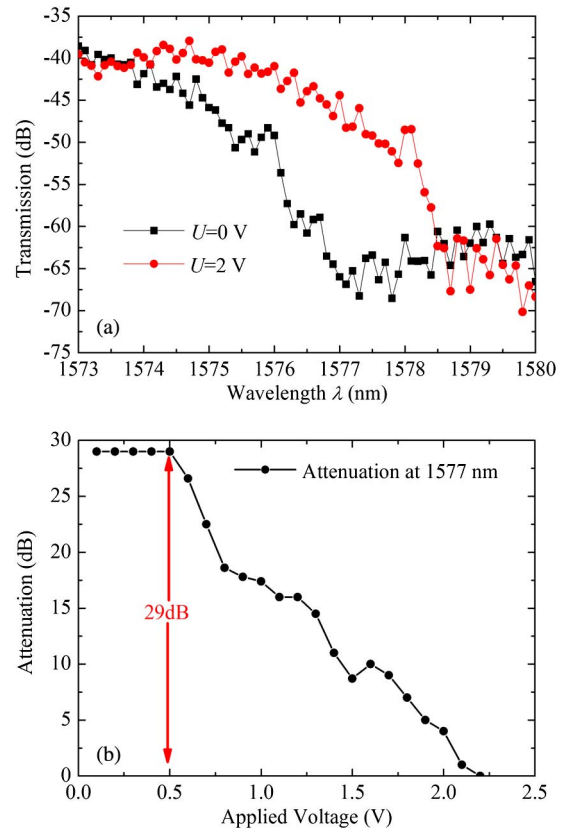
Fig. 9. (a) Transmission spectra of the VOA in 0 and 2 V applied voltage and (b) the attenuation characteristic of the VOA at 1577 nm.

In our experiment, the 2.2 V applied voltage refers to a power consumption of 43 mW.

Compared with the generally used VOAs on SOI platform, the proposed PCW-based VOA has only 1% of the generally device length, i.e., 16.8 μm, but performs comparable variable attenuation range (nearly 30 dB). In addition, the measured extinction ratio (maximum variable attenuation range) is also the largest in the reported tunable photonic devices to our knowledge.

4. Conclusions

In summary, we demonstrate a compact W1 PCW-based VOA with 16.8 μm length and 29 dB variable attenuation range at 1577 nm and the heating power of the VOA is less than 43 mW. The variation of the insertion loss and attenuation range of PCWs is optimized by different line-defect widths and r/a. Moreover, to reduce the insertion loss, a pair of five-period-long W1.2 LGI tapers is introduced between the W1 PCW and strip waveguide. Our results show that the proposed W1 PCW-based VOA is comparable with traditional VOAs in variable attenuation range, while the device length is only one percent of the traditional on-chip VOAs.

References

1. X. M. Zhang, A. Q. Liu, C. Lu, and D. Y. Tang, "MEMS variable optical attenuator using low driving voltage for DWDM systems," Electron. Lett. **38**, 382–383 (2002).
2. C. Lee, F. L. Hsiao, T. Kobayashi, K. H. Koh, P. V. Ramana, W. F. Xiang, B. Yang, C. W. Tan, and D. Pinjala, "A 1-V operated MEMS variable optical attenuator using piezoelectric PZT thin-film actuators," IEEE J. Sel. Top. Quantum Electron. **15**, 1529–1536 (2009).
3. S. M. Garner and S. Caracci, "Variable optical attenuator for large-scale integration," IEEE Photon. Technol. Lett. **14**, 1560–1562 (2002).
4. X. Q. Jiang, W. Qi, H. Zhang, Y. Tang, Y. L. Hao, J. Y. Yang, and M. H. Wang, "Low crosstalk 1×2 thermooptic digital optical switch with integrated S-bend attenuator," IEEE Photon. Technol. Lett. **18**, 610–612 (2006).
5. P. F. Qu, W. Y. Chen, F. M. Li, C. X. Liu, and W. Dong, "Analysis and design of thermo-optical variable optical attenuator using three-waveguide directional couplers based on SOI," Opt. Express **16**, 20334–20344 (2008).
6. M. I. Lapsley, S. Lin, X. L. Mao, and T. J. Huang, "An in-plane, variable optical attenuator using a fluid-based tunable reflective interface," Appl. Phys. Lett. **95**, 083507 (2009).
7. S. Park, T. Tsuchizawa, T. Watanabe, H. Shinojima, H. Nishi, K. Yamada, Y. Ishikawa, K. Wada, and S. Itabashi, "Monolithic integration and synchronous operation of germanium photodetectors and silicon variable optical attenuators," Opt. Express **18**, 8412–8421 (2010).
8. P. P. Sahu, "Variable optical attenuator using thermo-optic two-mode interference device with fast response time," Appl. Opt. **48**, 4213–4218 (2009).
9. T. Baba, "Slow light in photonic crystals," Nat. Photonics **2**, 465–473 (2008).
10. M. Notomi, K. Yamada, A. Shinya, J. Takahashi, C. Takahashi, and I. Yokohama, "Extremely large group-velocity dispersion of line-defect waveguides in photonic crystal slabs," Phys. Rev. Lett. **87**, 253902 (2001).
11. T. Chu, H. Yamada, S. Ishida, and Y. Arakawa, "Thermooptic switch based on photonic-crystal line-defect waveguides," IEEE Photon. Technol. Lett. **17**, 2083–2085 (2005).
12. L. L. Gu, W. Jiang, X. N. Chen, and R. T. Chen, "Thermooptically tuned photonic crystal waveguide silicon-on-insulator Mach–Zehnder interferometers," IEEE Photon. Technol. Lett. **19**, 342–344 (2007).
13. H. C. Nguyen, S. Hashimoto, M. Shinkawa, and T. Baba, "Compact and fast photonic crystal silicon optical modulators," Opt. Express **20**, 22465–22474 (2012).
14. D. M. Beggs, T. P. White, L. O'Faolain, and T. F. Krauss, "Ultracompact and low-power optical switch based on silicon photonic crystals," Opt. Lett. **33**, 147–149 (2008).
15. Y. H. Cui, K. Liu, D. L. MacFarlane, and J. B. Lee, "Thermo-optically tunable silicon photonic crystal light modulator," Opt. Lett. **35**, 3613–3615 (2010).
16. K. Cui, Q. Zhao, X. Feng, Y. Huang, Y. Li, D. Wang, and W. Zhang, "Thermo-optic switch based on transmission-dip shifting in a double-slot photonic crystal waveguide," Appl. Phys. Lett. **100**, 201102 (2012).
17. K. Cui, X. Feng, Y. Huang, Q. Zhao, Z. Huang, and W. Zhang, "Broadband switching functionality based on defect mode coupling in W2 photonic crystal waveguide," Appl. Phys. Lett. **101**, 151110 (2012).
18. Q. Zhao, K. Cui, Z. Huang, X. Feng, D. Zhang, F. Liu, W. Zhang, and Y. Huang, "Compact thermo-optic switch based on tapered W1 photonic crystal waveguide," IEEE Photon. J. **5**, 2200606 (2013).
19. X. Wang, S. Chakravarty, B. S. Lee, C. Lin, and R. T. Chen, "Ultraefficient control of light transmission through photonic potential barrier modulation," Opt. Lett. **34**, 3202–3204 (2009).
20. M. T. Tinker and J. B. Lee, "Thermo-optic photonic crystal light modulator," Appl. Phys. Lett. **86**, 221111 (2005).
21. M. T. Tinker and J. B. Lee, "Thermal and optical simulation of a photonic crystal light modulator based on the thermo-optic shift of the cut-off frequency," Opt. Express **13**, 7174–7188 (2005).
22. Q. Zhao, K. Cui, X. Feng, Y. Huang, Y. Li, D. Zhang, and W. Zhang, "Ultra-compact variable optical attenuator based on slow light photonic crystal waveguide," Chin. Opt. Lett. **11**, 031301 (2013).
23. A. Hosseini, X. C. Xu, D. N. Kwong, H. Subbaraman, W. Jiang, and R. T. Chen, "On the role of evanescent modes and group index tapering in slow light photonic crystal waveguide coupling efficiency," Appl. Phys. Lett. **98**, 031107 (2011).
24. K. Cui, Y. Huang, G. Zhang, Y. Li, X. Tang, X. Mao, Q. Zhao, W. Zhang, and J. Peng, "Temperature dependence of ministop band in double-slots photonic crystal waveguides," Appl. Phys. Lett. **95**, 191901 (2009).
25. S. Rahimi, A. Hosseini, X. C. Xu, H. Subbaraman, and R. T. Chen, "Group-index independent coupling to band engineered SOI photonic crystal waveguide with large slow-down factor," Opt. Express **19**, 21832–21841 (2011).
26. C. Y. Lin, X. L. Wang, S. Chakravarty, B. S. Lee, W. C. Lai, and R. T. Chen, "Wideband group velocity independent coupling into slow light silicon photonic crystal waveguide," Appl. Phys. Lett. **97**, 183302 (2010).